AIMS Mathematics, 7(6): 11399–11416.
DOI:10.3934/math.2022636
Received: 03 February 2022
Revised: 06 March 2022
Accepted: 13 March 2022
Published: 12 April 2022

http://www.aimspress.com/journal/Math

Research article

Global stability of local fractional Hénon-Lozi map using fixed point theory

Rabha W. Ibrahim [1,*] **and Dumitru Baleanu**[2,3,4]

[1] The Institute of Electrical and Electronics Engineers (IEEE): 94086547
[2] Department of Mathematics, Cankaya University, 06530 Balgat, Ankara, Turkey
[3] Institute of Space Sciences, R76900 Magurele-Bucharest, Romania
[4] Department of Medical Research, China Medical University, Taichung 40402, Taiwan

* **Correspondence:** Email: rabhaibrahim@yahoo.com.

Abstract: We present an innovative piecewise smooth mapping of the plane as a parametric discrete-time chaotic system that has robust chaos over a share of its significant organization parameters and includes the generalized Henon and Lozi schemes as two excesses and other arrangements as an evolution in between. To obtain the fractal Henon and Lozi system, the generalized Henon and Lozi system is defined by adopting the fractal idea (FHLS). The recommended system's dynamical performances are investigated from many angles, such as global stability in terms of the set of fixed points.

Keywords: fractional calculus; differential operator; fractional differential equation; fractal chaotic; fractal
Mathematics Subject Classification: 28D37, 30D05

1. Introduction

Because the presence of these windows in certain chaotic areas implies that small changes in the parameters will end the chaos, the resilient chaotic system (map) is defined by the absence of episodic windows and simultaneous attractors in some parameter space neighborhood. This outcome reflects the fragile nature of this form of chaos. The chaotic dynamical system has been studied extensively by many academics because to its wide applications in science and engineering. The first discrete-time chaotic system [1] was suggested by H'enon. Lozi developed a unique discrete chaotic system utilizing the quadratic formula in the H'enon map with quasi linear term [2]. To improve the map in [3], it is advised to use a linear combination (convex type) of H'enon and Lozi maps. The H'enon-Lozi system has recently been developed using fractional calculus and the Capotu derivative operator in [4] and its extensions.

The notion of local fractional calculus (fractal calculus), first introduced by Kolwankar and Gangal for the regular fractional operators of Riemann-Liouville calculus [5, 6]. It was used to deal with non-differentiable formulas that appeared in engineering sciences, thermal and heat transforms another science [6–8]. Various other ideas and specifics of fractal calculus were introduced, such as the geometric fractal. In the logical extensions of the definitions to the issue of local derivative on fractals, Yang et al. [6] constructed what is known as the cantor fractal.

Recognition of patterns using the fractal concept has been increased in the last decay. In [9], the authors joined procedure of altered edge detection techniques with box-counting for fractal feature extraction. Edge detection of fractal images can be studied as a significant area of investigation in fractal image processing [10]. License plate recognition is an emerging concept for real-time applications, is improved by using a new fractal series expansion [11]. Fractal entropy is developed and used in [12]. Finally, it employed to analyze images [13]. In this note, we use the fractal difference operator to define a new fractal Hénon-Lozi system (fractal map (FHLS)). Employing the FHLS to study the image recognition. Other studies are presented in [14–32].

To spread between the asymptotically stable variety and the chaotic array, we analyze bifurcation diagrams and present new irregular limitations on the fractal order. Utilizing bifurcation maps produced using forward and backward extension procedures, domains of fractal order spaces are confirmed, and the existence of simultaneous is demonstrated.

The paper is organized as follows: Section 2 deals with methods that we utilize in the sequel, Section 3 involves the main conditions for the global stability, Section 4 produces the test of our results and Section 5 indicates the conclusion.

2. Methodology

In this section, we illustrate our methodology based on the fractal concept.

2.1. Fractal concept

Let $C_\alpha(a, b), \alpha \in (0, 1]$ be a fractal set and let $f \in C_\alpha$. For $\varepsilon > 0$ and $|\chi - \chi_0| < \delta$, the limit

$$f^{(\alpha)}(\chi) := \eth^{(\alpha)} f(\chi) = \lim_{\chi \to \chi_0} \frac{\Gamma(\alpha + 1)(f(\chi) - f(\chi_0))}{(\chi - \chi_0)^\alpha}$$

is finite and available. It indicates that

$$f^{(2\alpha)}(\chi) = (f^{(\alpha)})^{(\alpha)}(\chi),\ f^{(3\alpha)}(\chi) = ((f^{(\alpha)})^{(\alpha)})^{(\alpha)}(\chi)...$$

The 2D-fractal differential operator is presented for $f(x, y)$ defining on the space of fractal C_α in x-direction

$$\eth_x^{(\alpha)} f(x, y) = \lim_{x \to x_0} \frac{\Gamma(\alpha + 1)(f(x, y) - f(x_0, y))}{(x - x_0)^\alpha},$$

and in y-direction

$$\eth_y^{(\alpha)} f(x, y) = \lim_{y \to y_0} \frac{\Gamma(\alpha + 1)(f(x, y) - f(x, y_0))}{(y - y_0)^\alpha},$$

For example,

$$f(x^\alpha, y^\alpha) = x^{\alpha n} y^{n\alpha}$$

has the following fractal derivatives

$$\begin{aligned} \eth_x^{(\alpha)} x^{n\alpha} y^{n\alpha} &= \left(\frac{\Gamma(\alpha n + 1)}{\Gamma(\alpha(n-1)+1)} x^{(n-1)\alpha} \right) y^{n\alpha}, \\ \eth_y^{(\alpha)} x^{n\alpha} y^{n\alpha} &= \left(\frac{\Gamma(\alpha n + 1)}{\Gamma(\alpha(n-1)+1)} y^{(n-1)\alpha} \right) x^{n\alpha}, \end{aligned} \tag{2.1}$$

respectively. The results of Eq (2.1) are two vectors, one represents the fractal derivative of the image pixel in x-direction and the second one indicates the fractal derivative of the image pixel in y-direction. Note that the fractal difference term is in p.15 of [6].

$$\triangle^{\alpha} f(x) = \Gamma(1+\alpha)[f(x) - f(x_0)].$$

Moreover, the definition of fractal integral is in p.38 of [6], as follows:

$$\Im^{\alpha} f(x) = \frac{1}{\Gamma(1+\alpha)} \sum_{j=0}^{n} \lim_{\delta(x_j)\to 0} \left(f(x_j)\delta^{\alpha}(x_j) \right),$$

where $\delta(x_j)$ is a small number that indicates the difference between the modeled map and the real data. More knowledge about fractal trigonometric functions is the fractal sine function

$$\sin_{\alpha}(\chi^{\alpha}) = \sum_{m=0}^{\infty} \frac{(-1)^m \chi^{(2m+1)\alpha}}{\Gamma\left(1 + (2m+1)\alpha\right)}, \quad \alpha \in (0,1),$$

and the fractal cosine function

$$\cos_{\alpha}(\chi^{\alpha}) = \sum_{m=0}^{\infty} \frac{(-1)^m \chi^{2m\alpha}}{\Gamma\left(1 + 2m\alpha\right)}, \quad \alpha \in (0,1).$$

2.2. Fractal Hénon-Lozi system (FHLS)

The Hénon system formulates a point (x_n, y_n) in the plane and translates it to a new position (point) [1]

$$\begin{cases} x_{n+1} = 1 - \wp\, x_n^2 + y_n, \\ y_{n+1} = \ell\, x_n, \end{cases}$$

while the Lozi system indicates the following formula [2]

$$\begin{cases} x_{n+1} = 1 - \wp\, |x|_n + y_n, \\ y_{n+1} = \ell\, x_n. \end{cases}$$

Considering the function

$$\hbar_{\mathbb{k}}(x) = \mathbb{k}|x| + (1-\mathbb{k})x^2, \mathbb{k} \in [0,1],$$

the following Hénon-Lozi system is recognized by [3]

$$\begin{cases} x_{n+1} = 1 - \wp\, \hbar_{\mathbb{k}}(x_n) + y_n, \\ y_{n+1} = \ell\, x_n. \end{cases}$$

Assuming the difference operator $\Delta x_n = x_{n+1} - x_n$, we obtain the difference system

$$\begin{cases} \Delta x_n = (1 - \wp\, \hbar_{\Bbbk}(x_n) + y_n - x_n)\,, \\ \Delta y_n = (\ell\, x_n - y_n)\,. \end{cases} \tag{2.2}$$

Utilizing the fractal difference operator Δ^{α}, we have FHLS

$$\begin{cases} \Delta^{\alpha} x_n = (1 - \wp\, \hbar_{\Bbbk}(x_n) + y_n - x_n)\,\Gamma(1+\alpha), \\ \Delta^{\alpha} y_n = (\ell\, x_n - y_n)\,\Gamma(1+\alpha). \end{cases} \tag{2.3}$$

We present the next outcome.

Proposition 1. *Consider FHLS in* (2.3)*. Then*

- *the solution is determined by the fractal integral system*

$$\begin{cases} x_n = \dfrac{1}{\Gamma(1+\alpha)} \sum_{j=0}^{n-1} \left(1 - \wp\, \hbar_{\Bbbk}(x_j) + y_j - x_j\right), \\ y_n = \dfrac{1}{\Gamma(1+\alpha)} \sum_{j=0}^{n-1} \left(\ell\, x_j - y_j\right); \end{cases}$$

- *the critical points are*

$$x_n = -\frac{\sqrt{(\ell - 1 - \wp\Bbbk)^2 - 4\,(\wp(1-\Bbbk))} + (\ell - 1 - \wp\Bbbk)}{2\,(\wp(1-\Bbbk))}, \wp(1-\Bbbk) \neq 0, y_n = \ell x_n$$

and

$$x_n = \frac{\sqrt{(\ell - 1 - \wp\Bbbk)^2 - 4\,(\wp(1-\Bbbk))} - (\ell - 1 - \wp\Bbbk)}{2\,(\wp(1-\Bbbk))}, \wp(1-\Bbbk) \neq 0, y_n = \ell x_n$$

- *the eigenvalues and eigenvectors of the Jacobian matrix of* (2.3) *are*

$$\lambda_1 = \frac{\Gamma(1+\alpha)}{2} \times$$
$$\left(-\sqrt{(\wp(2(1-\Bbbk)x_n + \Bbbk)^2 + 2\wp(2(1-\Bbbk)x_n + \Bbbk) + 4\ell + 1)} + \wp(2(1-\Bbbk)x_n + \Bbbk) - 1\right)$$
$$\lambda_2 = \frac{\Gamma(1+\alpha)}{2}$$
$$\left(\sqrt{(\wp(2(1-\Bbbk)x_n + \Bbbk)^2 + 2\wp(2(1-\Bbbk)x_n + \Bbbk) + 4\ell + 1)} + \wp(2(1-\Bbbk)x_n + \Bbbk) - 1\right)$$
$$v_1 = \Gamma(1+\alpha) \times$$
$$\left(-\frac{(-1 - \wp(\Bbbk + 2(1-\Bbbk)x_n) + \sqrt{(1 + 4\ell + 2\wp(\Bbbk + 2(1-\Bbbk)x_n) + \wp(\Bbbk + 2(1-\Bbbk)x_n)^2))}}{2\ell}, 1\right)$$
$$v_2 = \Gamma(1+\alpha) \times$$
$$\left(-\frac{(-1 - \wp(\Bbbk + 2(1-\Bbbk)x_n) - \sqrt{(1 + 4\ell + 2\wp(\Bbbk + 2(1-\Bbbk)x_n) + \wp(\Bbbk + 2(1-\Bbbk)x_n)^2))}}{2\ell}, 1\right)$$

- *the values of $\lambda_{1,2}$ can be approximated in terms of x_n as follows:*

$$\begin{aligned}\lambda_{1,2} = &\frac{\Gamma(1+\alpha)}{2}\\ &\pm\Big(\sqrt{(\wp\left(\frac{((1-\Bbbk)(\sqrt{(a^2-4b)}\pm a))}{b}+\Bbbk\right)^2}\\ &+\sqrt{2\wp\left(\frac{((1-\Bbbk)(\sqrt{(a^2-4b)}\pm a))}{b}+\Bbbk\right)+4\ell+1)}\Big)\\ &+\frac{\Gamma(1+\alpha)}{2}\left(\wp\left(\frac{((1-\Bbbk)(\sqrt{(a^2-4b)}\pm a))}{b}+\Bbbk\right)-1\right),\end{aligned}$$

where $a = \ell - 1 - \wp\Bbbk$ and $b = \wp(1-\Bbbk)$.

Proof. Applying the definition of fractal integral on the system FHLS in (2.3), we directly obtain the desired result, when $\delta_j^\alpha = 1$. For the second part, substitute $y = \ell x$ in the first equation, we have

$$1 + x(\ell - 1 - \wp\Bbbk) + \wp(1-\Bbbk)x^2 = 0,$$

which has two solutions when $\wp(1-\Bbbk) \neq 0$. The third assertion is a direct application of the Jacobian matrix, while the last is a substitution of the values of the critical points in the values of the eigenvalues. □

Example 1. *We illustrate our example, as follow:*

- *Consider the following data $\wp = 1, \Bbbk = 0.5, \ell = 0.3$ then we have $a = -1.2$ and $b = 0.5$. A computation yields $\lambda_{1,2} = \Gamma(1+\alpha)(\pm 1.04)$.*
- *Consider the following data $\wp = 1, \Bbbk = 0.3, \ell = 0.3$ then we have $a = -1.0$ and $b = 0.7$. A computation yields $\lambda_{1,2} = \Gamma(1+\alpha)(\pm 1.00)$.*
- *Consider the following data $\wp = 2, \Bbbk = 0.3, \ell = 0.3$ then we have $a = -1.0$ and $b = 0.7$. A computation yields $\lambda_{1,2} = \Gamma(1+\alpha)(\pm 1.09)$.*
- *Consider the following data $\wp = 3, \Bbbk = 0.3, \ell = 0.3$ then we have $a = -1.0$ and $b = 0.7$. A computation yields $\lambda_{1,2} = \Gamma(1+\alpha)(\pm 1.095)$.*

From the above example, for $\ell = 0.3, \Bbbk \in [0,1]$ and for a positive constant $\wp < \infty$, we conclude that $\lambda_{1,2} \approx \pm\Gamma(1+\alpha)$. That is the eigenvalues depend on the fractal number $\alpha \in [0,1]$. Also, around $\alpha = 0$, we have

$$\begin{aligned}\lambda_{1,2} \approx \pm\Big(&1 - \gamma\alpha + 1/12(6\gamma^2 + \pi^2)\alpha^2 + 1/6\alpha^3(-\gamma^3 - (\gamma\pi^2)/2 + \psi(2,1))\\ &+ 1/24\alpha^4(\gamma^4 + \gamma^2\pi^2 + (3\pi^4)/20 - 4\gamma\psi(2,1)) + O(\alpha^5)\Big),\end{aligned}$$

where $\gamma = 0.577$ presents the Euler constant and ψ indicates the digamma function. Figure 1 shows the behavior of $\lambda_{1,2}$ with the arch curve length

$$\int_0^1 \sqrt{(1 + \Gamma(1+\alpha)^2\psi(0, 1+\alpha)^2)}d\alpha \approx 1.03513728337393...$$

Some examples are illustrated in Figure 2.

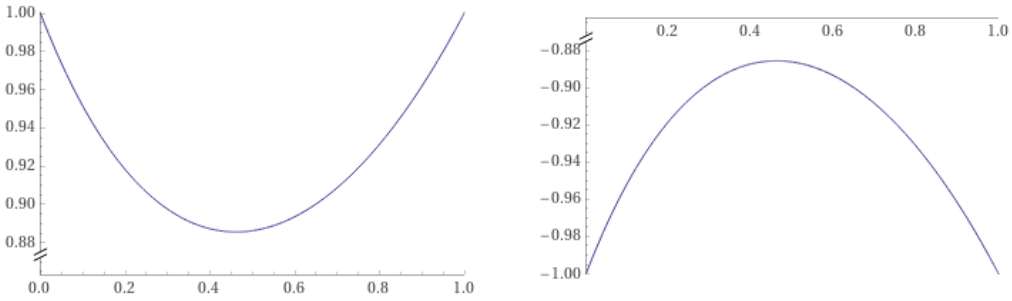

Figure 1. The plot of $\lambda_{1,2}$ respectively, where $\alpha = 0.461632$ is the value of the extreme point of $\lambda_{1,2}$.

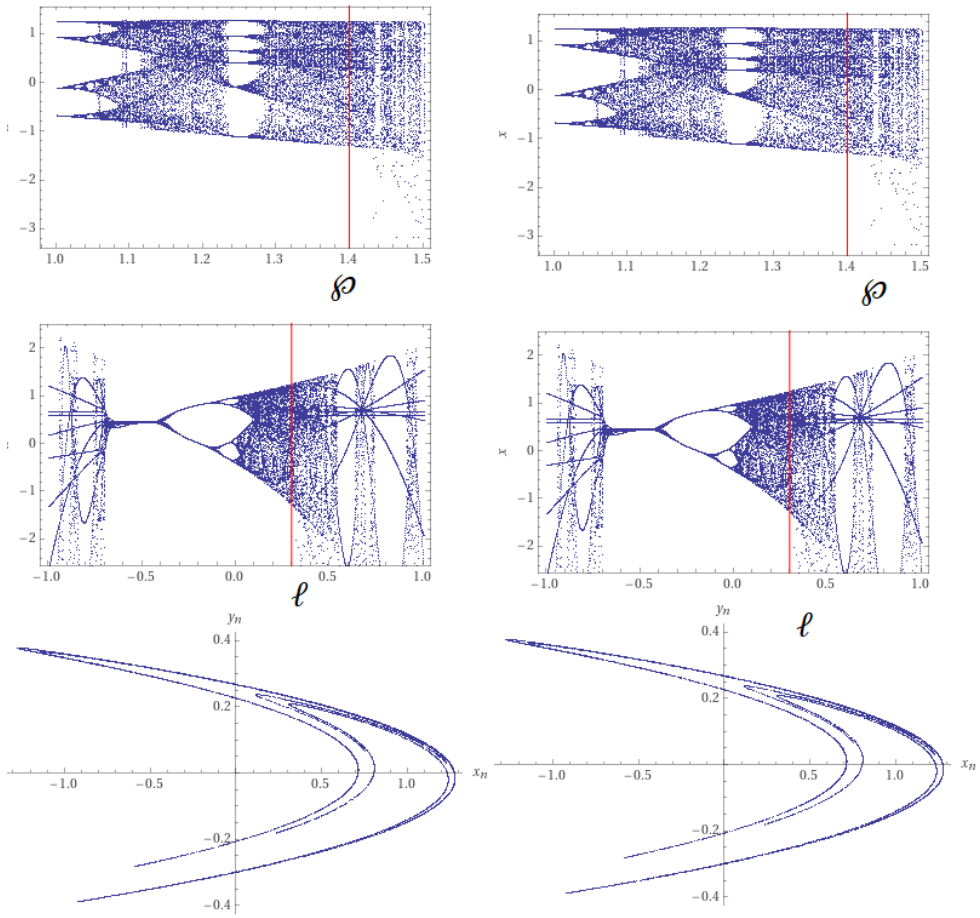

Figure 2. The behavior of System (2.3), when $\wp = 1.4, \ell = 0.3, \alpha = 0.4616$ and initial values (0.0) in the first column and (1/2,1/2) in the second column respectively; the fractional power is taken when its value at the extreme point of $\lambda_{1,2}$.

2.3. Chaotic system that involves FHLS

Because the presence of cyclic windows (periodic) in various chaotic indicators implies that even minor modifications in the parameters will destroy the chaos, robust chaos is defined by the absence of cycling values and coexisting attractors in a particular region of the parameter space. This impact hints at the vulnerability of this kind of disorder. Despite this, there are numerous functional applications where trustworthy chaotic mode operation is essential, such as connections and spreading the spectrum of switch-mode power supplies to avert electromagnetic interference. There are different methods to investigate robust chaos such as using polynomials, one parametric system, multi-parametric system [14, 15].

There are two considerations of the chaotic system with robust chaos in $[0, 1]$ corresponding to FHLS (C-FHLS): 1D-parameter C-FHLS, which presents by letting $\alpha = \Bbbk \in [0, 1]$, and 2D-parameter C-FHLS, which indicates two different values of $\alpha \neq \Bbbk \in [0, 1]$.

We shall study the two cases.

2.3.1. 1D-parameter C-FHLS

In this case, the C-FHLS is given by the formula

$$\Upsilon_\alpha(x, y) = \begin{pmatrix} (1 - \wp\, \hbar_\alpha(x) + y - x)\, \Gamma(1 + \alpha) \\ (\ell\, x - y)\, \Gamma(1 + \alpha) \end{pmatrix} \quad \alpha \in [0, 1], \tag{2.4}$$

where α indicates the bifurcation parameter achieving the functional $\hbar_\alpha(x) = \alpha|x| + (1 - \alpha)x^2$. It is clear that when $\alpha = 0, \wp = 1.4$ and $\ell = 0.3$, we have the difference Henon map and for $\alpha = 1$, we get the difference Lozi map. It's worth noting that we get the chaotic map satisfying various forms of attractors for $\alpha \in (0, 1)$. Figure 2 shows the Lyapunov exponents and bifurcation diagram. The structure (see Figure 3) can be used to express the Lyapunov exponents.

$$V = \lim_{n\to\infty} \frac{1}{n} \ln \left|\lambda_{1,2}^n\right|,$$

where $\lambda_{1,2}$ are the eigenvalues of the Jacobi matrix of (2.4),

$$J_\alpha = \begin{pmatrix} (-\wp\, \hbar'_\alpha(x) - 1)\, \Gamma(1 + \alpha) & \Gamma(1 + \alpha) \\ \ell\Gamma(1 + \alpha) & -\Gamma(1 + \alpha) \end{pmatrix}.$$

There are two different eigenvalues

$$\lambda_{1,2} = \frac{\Gamma(\alpha + 1)}{10} \left(\pm \sqrt{196\alpha^2x^2 + 196\alpha^2x + 49\alpha^2 - 336\alpha x - 168\alpha + 174} - 14\alpha x - 7\alpha + 2 \right). \tag{2.5}$$

We note that the chaotic map Υ_α is a piecewise smooth map, and that $\alpha \in [0, 1]$ will be partitioned into two domains in accordance with the shape of the chaotic map Υ_α.

$$R_1 := \Big\{ (x, y) \in \mathbb{R}^2 : \alpha - 1 \neq 0, x = \frac{\sqrt{7}\, \sqrt{28\alpha^2 - 52\alpha + 87} + 14\alpha + 7}{28(\alpha - 1)} < 0,$$
$$y = \frac{3(\sqrt{7}\, \sqrt{28\alpha^2 - 52\alpha + 87} + 14\alpha + 7)}{280(\alpha - 1)} < 0 \Big\}$$

$$R_2 := \Big\{(x,y) \in \mathbb{R}^2 : \alpha - 1 \neq 0, x = \frac{-\sqrt{7}\sqrt{28\alpha^2 - 52\alpha + 87} + 14\alpha + 7}{28(\alpha - 1)} > 0,$$
$$y = \frac{3(-\sqrt{7}\sqrt{28\alpha^2 - 52\alpha + 87} + 14\alpha + 7)}{280(\alpha - 1)} > 0\Big\},$$

where $x = 0$ is a line equation that divides the phase plane into two domains R_1 and R_2. Note that, for $\alpha = 1$, we have the solution $(x = \frac{10}{21}, y = \frac{1}{7})$.

When $\alpha \in [0, 1]$, System (2.4) is obviously chaotic. Furthermore, in System (2.4), the control parameter α reveals the transition of dynamical performances from the Henon to the Lozi attractors. Lastly, System (2.4) indicates the robust chaotic attractors for $\alpha \in [0.4616, 1)$ and absent when $\alpha = 1$ and $\alpha = 0$.

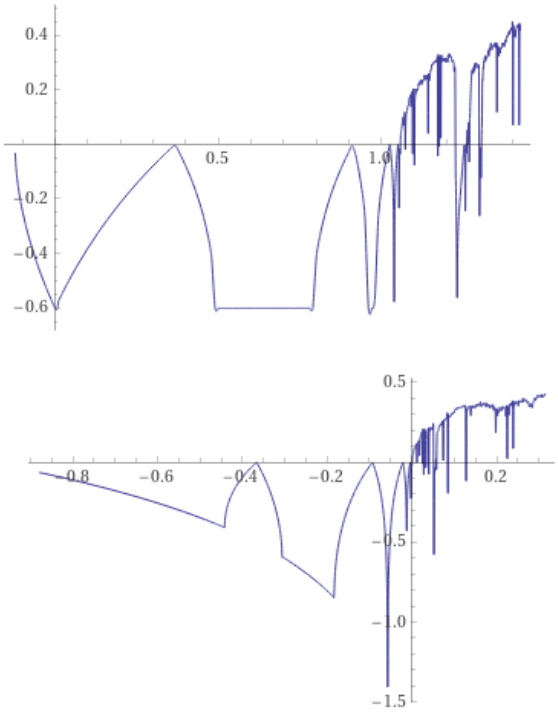

Figure 3. Maximum Lyapunov exponents $\eth = 0.418 \simeq \alpha$. The left graph is $(\wp, \eth)$ for fixed $\ell = 0.3$ and the right graph is $(\ell, \eth)$ for fixed $\wp = 1.4$.

2.3.2. 2D-parameter C-FHLS

In this part, we consider 2D-parameter C-FHLS $(\alpha, \Bbbk)$, where $\alpha \neq \Bbbk$ in $[0, 1]$. The system becomes

$$\Upsilon_{\alpha,\Bbbk}(x,y) = \begin{pmatrix} (1 - \wp\, \hbar_{\Bbbk}(x) + y - x)\,\Gamma(1+\alpha) \\ (\ell\, x - y)\,\Gamma(1+\alpha) \end{pmatrix} \quad \alpha, \Bbbk \in [0,1], \tag{2.6}$$

where α and $\Bbbk$ present the bifurcation parameters satisfying the functional

$$\hbar_{\Bbbk}(x) = \Bbbk|x| + (1 - \Bbbk)x^2,\ \Bbbk \in [0,1].$$

Eventually, for all $\alpha \in [0,1]$, The vector field of the chaotic map $\Upsilon_{\alpha,\Bbbk}$ owns two domains symbolized by:

$$D_1 := \Big\{(x,y) \in \mathbb{R}^2 : \Bbbk - 1 \neq 0, x = \frac{\sqrt{7}\,\sqrt{28\Bbbk^2 - 52\Bbbk + 87} + 14\Bbbk + 7}{28(\Bbbk - 1)} < 0,$$
$$y = \frac{3(\sqrt{7}\,\sqrt{28\Bbbk^2 - 52\Bbbk + 87} + 14\Bbbk + 7)}{280(\Bbbk - 1)} < 0\Big\}$$
$$D_2 := \Big\{(x,y) \in \mathbb{R}^2 : \Bbbk - 1 \neq 0, x = \frac{-\sqrt{7}\,\sqrt{28\Bbbk^2 - 52\Bbbk + 87} + 14\Bbbk + 7}{28(\Bbbk - 1)} > 0,$$
$$y = \frac{3(-\sqrt{7}\,\sqrt{28\Bbbk^2 - 52\Bbbk + 87} + 14\Bbbk + 7)}{280(\Bbbk - 1)} > 0\Big\}$$

where $x = 0$ is separated the plane into tow domains defining by D_1 and D_2. Putting $\alpha = 0.4616$ then $\Gamma(1.4616) = 0.88$ and hence we obtain $\hbar_{\Bbbk} \approx 1$ if and only if

$$x = \frac{5\Bbbk \pm \sqrt{5}\,\sqrt{5\Bbbk^2 - 22\Bbbk + 22}}{10(\Bbbk - 1)}, \Bbbk \neq 1.$$

By the above analysis, together with $\wp = 1.4$ and $\ell = 0.3$, we obtain the traditional Heno-Lozi system. This is true for all $\alpha \in [0.4616, 1]$. The Jacobian matrix is given by the formula

$$J_{\alpha,\Bbbk} = \begin{pmatrix} \Big(-\wp\,\hbar'_{\Bbbk}(x) - 1\Big)\Gamma(1+\alpha) & \Gamma(1+\alpha) \\ \ell\Gamma(1+\alpha) & -\Gamma(1+\alpha) \end{pmatrix}.$$

with two different eigenvalues (see Figures 4 and 5)

$$\lambda_{1,2} = \frac{\Gamma(\alpha+1)}{10}\Big(\pm\sqrt{196\Bbbk^2x^2 + 196\Bbbk^2x + 49\Bbbk^2 - 336\Bbbk x - 168\Bbbk + 174} - 14\Bbbk x - 7\Bbbk + 2\Big). \tag{2.7}$$

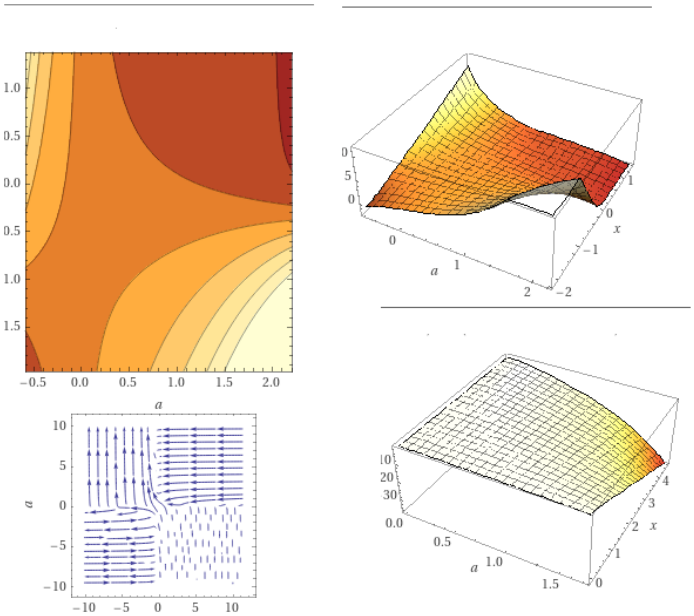

Figure 4. The plot of $\lambda_{1,2}$ respectively of J_α.

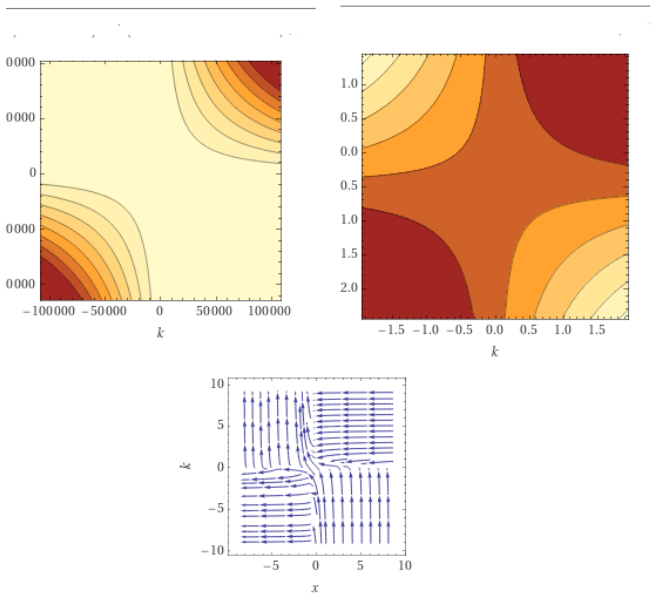

Figure 5. The plot of $\lambda_{1,2}$ respectively of $J_{0.4616,\Bbbk}$.

3. Global stability

In this section, we investigate the stability of the suggested system. To study this fact, we check the solution under the existing of the fixed points.

3.1. The set of the fixed points

For 1D-parameter C-FHLS, we have two fixed points when $\alpha = 0.4616$, as follows:

$$F_\alpha = \Big\{P_1(x = -3.8406, y = -0.541139),\ P_2(x = 0.345436, y = 0.0486719)\Big\},$$

where $P_1 \in R_1$ and $P_2 \in R_2$. Then Eq (2.5) yields

$$\begin{aligned}\lambda_{1,2}(P_1) =& \sqrt{196(-3.8)^2 * 0.4616^2 + 196 * (-3.8) * 0.4616^2}\\ &+ \sqrt{49 * 0.4616^2 - 336(-3.8 * 0.4616) - 168 * 0.4616 + 174}\\ &- 14(-3.8 * 0.4616) - 7 * 0.4616 + 2\\ &\approx 0.0843658415(\pm 57.0989...),\end{aligned}$$

where in $\lambda(P_1) = -57 \in R_1$. Similarly, we calculate the eigenvalues in R_2 to obtain

$$\begin{aligned}\lambda_{1,2}(P_2) =& \sqrt{196(0.3)^2 * 0.4616^2 + 196 * (0.3) * 0.4616^2}\\ &+ \sqrt{49 * 0.4616^2 - 336(0.3 * 0.4616) - 168 * 0.4616 + 174}\\ &- 14(0.3 * 0.4616) - 7 * 0.4616 + 2\\ &\approx 0.0843658415(\pm 5.58508...),\end{aligned}$$

thus, we have $\lambda(P_2) = 5.68 \in R_2$.

Obviously, the true solutions of the system are the fixed points of the unified chaotic map (2.4)

$$\begin{pmatrix} x \\ y \end{pmatrix} = \begin{pmatrix} (1 - \wp\, \hbar_\alpha(x) + y - x)\,\Gamma(1+\alpha) \\ (\ell\, x - y)\,\Gamma(1+\alpha) \end{pmatrix}, \quad \alpha \in [0,1]. \tag{3.1}$$

For the 2D-parameter C-FHLS, we have the following set of fixed points

$$\begin{aligned} F_{\alpha,\Bbbk} = \Big\{ & Q_1(x = 0.295136,\ y = 0.0415845), \\ & Q_2(x = \frac{1}{\Bbbk - 1}(0.5\Bbbk + 0.7), y = \frac{1}{\Bbbk - 1}(0.07\Bbbk + 0.1)) \Big\}, \quad \Bbbk \in (0,1), \end{aligned}$$

where $Q_1 \in D_2$ and $Q_2 \in D_1$. Consequently, we get

$$\lambda_{1,2}(Q_1) = \frac{\Gamma(\alpha+1)}{10} \pm \sqrt{125.44\Bbbk^2 - 268.8\Bbbk + 174} - 11.2\Bbbk + 2 \in D_2, \quad \forall \alpha \in (0,1),$$

which indicates the root $\Bbbk = \dfrac{85}{112}$.

Moreover, for the second fixed point, we have

$$\lambda_{1,2}(Q_2) = \frac{\Gamma(\alpha+1)}{10} \pm \sqrt{2}\sqrt{\frac{(98\Bbbk^4 - 168\Bbbk^3 + 255\Bbbk^2 - 174\Bbbk + 87)}{(\Bbbk - 1)^2)}} - 14\Bbbk - \frac{14}{(\Bbbk - 1)} - 12.$$

It is clear that $0 < \Bbbk < 1$, implies

$$\lambda(Q_2) = 0.1 - \sqrt{2}\sqrt{\frac{(98\Bbbk^4 - 168\Bbbk^3 + 255\Bbbk^2 - 174\Bbbk + 87)}{(\Bbbk - 1)^2}} - 14\Bbbk - \frac{14}{(\Bbbk - 1)} - 12 < 0,$$

which leads to $\lambda(Q_2) \in D_1$. Clearly, the true solutions of the system are the fixed points of the unified chaotic map (2.6)

$$\begin{pmatrix} x \\ y \end{pmatrix} = \begin{pmatrix} (1 - \wp\, \hbar_\Bbbk(x) + y - x)\,\Gamma(1+\alpha) \\ (\ell\, x - y)\,\Gamma(1+\alpha) \end{pmatrix} \quad \alpha, \Bbbk \in [0,1], \tag{3.2}$$

The next section deals with the stability conditions and global stability using the set of fixed points.

3.2. Stability

The goal of this section is to look into the stability of the suggested systems.

Definition 1. *Let χ be a solution of the fractal equation*

$$\Delta^\alpha \chi(t) = \varphi(t, \chi), \quad t \in [t_0, \infty)$$

such that $\|\chi\| < t_0$. Then χ is called stable solution if there occurs a positive constant $\varrho > 0$ for all solution χ_1 satisfying $\|\chi_1 - \chi_0\| < \varrho$ and given $\rho > 0$ there occurs $0 < \delta \leq \varrho$ such that

$$\|\chi_1 - \chi_0\| < \delta \Rightarrow$$

$$\|\chi(t,t_0,\chi_1)-\chi(t,t_0,\chi_0)\|\leq\rho,\quad t_0\leq t<\infty.$$

Moreover, if

$$\lim_{t\to\infty}\|\chi(t,t_0,\chi_1)-\chi(t,t_0,\chi_0)\|=0$$

then χ is asymptotically stable.

The following are the outcomes:

Theorem 2. *All solutions of the continuous linear system corresponding to* (2.4) *(similarly for* (2.6)*)*

$$\mathfrak{d}^{(\alpha)}\begin{pmatrix}x(t)\\y(t)\end{pmatrix}=\Lambda_{2\times2}(t)\begin{pmatrix}x(t)\\y(t)\end{pmatrix}\tag{3.3}$$

are stable if and only if they are bounded. In addition, if the characteristic polynomial of Λ is stable then the solutions are asymptotically stable.

Proof. Let's start by defining a two-variable matrix-valued function, which we'll call Θ as follows:

$$\Theta(t,t_0)=\Im+\mathfrak{I}^{\alpha}\Lambda(t)+\mathfrak{I}^{\alpha}\Lambda(\delta_1^{\alpha})+...+\mathfrak{I}^{\alpha}\Lambda(\delta_{n-1}^{\alpha}),$$

where $\Im$ is the identity matrix. By the formula of $\mathfrak{I}^{\alpha}$, we obtain

$$\Theta(t,t_0)=\Im.$$

If all solutions of System (3.3) are bounded, then there is a constant $\sigma>0$ such that the fundamental matrix of (3.3) satisfies $\|\Theta\|<\sigma$, where $\|.\|$ indicates the max norm. That is

$$\|x(t)-x_0(t)\|<\frac{\rho}{2\sigma},\quad \|y(t)-y_0(t)\|<\frac{\rho}{2\sigma},\quad \rho>0.$$

Since the solution of (3.3) achieves

$$X(t)=\Theta(t,t_0)X_0(t),\quad X=(x\ y)^{\top}.$$

Then a computation implies

$$\begin{aligned}\|X(t)-X_0(t)\|&\leq\|\Theta\left(X(t)-X_0(t)\right)\|\\&\leq\sigma\|X(t)-X_0(t)\|\\&<\sigma(\frac{\rho}{2\sigma}+\frac{\rho}{2\sigma})\\&=\rho.\end{aligned}$$

Therefore, all the outcomes are stable.

Conversely, the stability of the solutions brings that there occurs $\eta>0$ corresponding to a given $\kappa>0$ such that

$$\|X(t)\|<\eta\Rightarrow\|\Theta(t)X_0(t)\|<\kappa\|X_0(t)\|.$$

That is all solutions are bounded.

The second part of the theorem, can be realized by the conclusion, which is an extended of Eq (1.9) in [6],

$$\begin{aligned}\|X(t)-X_0(t)\|&\leq\sigma\exp(-\rho(t^{\alpha}))\|X(t)-X_0(t)\|\\&=0,\quad t\to\infty,\end{aligned}$$

which leads to asymptotically stable solutions. □

In the similar manner of Theorem 2, we have the following result

Theorem 3. *All solutions of the continuous nonlinear system corresponding to* (2.4) *(similarly for* (2.6)*)*

$$\eth^{(\alpha)}\begin{pmatrix}x(t)\\y(t)\end{pmatrix} = \Lambda_{2\times 2}(t)\begin{pmatrix}x(t)\\y(t)\end{pmatrix} + \begin{pmatrix}\Sigma_1(t)\\\Sigma_2(t)\end{pmatrix} \tag{3.4}$$

are stable if and only if they are bounded and

$$\|\Sigma\| < \varsigma,\ \varsigma \in (0,\infty), \Sigma = (\Sigma_1, \Sigma_2)^\top.$$

In addition, if the characteristic polynomial of Λ *is stable then the solutions are asymptotically stable.*

3.3. Stabilization control

In this section, we'll discuss how to use control laws to stabilize the fractal map seen above.

Theorem 4. *Under the 1D-control law, the 1D-parameter fractal map*

$$\begin{cases}\Delta^\alpha x(t) = (1 - \wp\, \hbar_\alpha(x(t)) + y(t) - x(t))\,\Gamma(1+\alpha),\\ \Delta^\alpha y(t) = (\ell\, x(t) - y(t))\,\Gamma(1+\alpha).\end{cases} \tag{3.5}$$

can be controlled by

$$U_x(t) = (\wp\hbar_\alpha(x) - y - 1)\,\Gamma(1+\alpha), \quad \alpha \in [0,1] \tag{3.6}$$

Proof. The time-varying control parameter $U_x(t)$ is utilized in the controlled fractional order Henon-Lozi map, which is defined as

$$\begin{cases}\Delta^\alpha x(t) = (1 - \wp\, \hbar_\alpha(x(t)) + y(t) - x(t))\,\Gamma(1+\alpha) + U_x(t),\\ \Delta^\alpha y(t) = (\ell\, x(t) - y(t))\,\Gamma(1+\alpha).\end{cases} \tag{3.7}$$

This yields the system

$$\begin{cases}\Delta^\alpha x(t) = (-x(t))\,\Gamma(1+\alpha),\\ \Delta^\alpha y(t) = (\ell\, x(t) - y(t))\,\Gamma(1+\alpha).\end{cases} \tag{3.8}$$

In matrix form, we get

$$\Delta^\alpha\begin{pmatrix}x(t)\\y(t)\end{pmatrix} = \begin{pmatrix}-\Gamma(1+\alpha) & 0\\ \ell\Gamma(1+\alpha) & -\Gamma(1+\alpha)\end{pmatrix}\begin{pmatrix}x(t)\\y(t)\end{pmatrix}. \tag{3.9}$$

The eigenvalues corresponding to (3.9) are $\lambda_1 = \lambda_2 = -\Gamma(1+\alpha)$. Thus, the zero solution of (3.9) is bounded. According to Theorem 2, the zero solution is asymptotically stable, and so the system is stabilized. □

We get the following outcome from the same conclusion.

Theorem 5. *The 2D- parameter fractal map*

$$\begin{cases}\Delta^\alpha x(t) = (1 - \wp\, \hbar_{\Bbbk}(x(t)) + y(t) - x(t))\,\Gamma(1+\alpha),\\ \Delta^\alpha y(t) = (\ell\, x(t) - y(t))\,\Gamma(1+\alpha),\end{cases} \tag{3.10}$$

can be governed by the 1D-control legislation

$$W_x(t) = (\wp\hbar_{\Bbbk}(x) - y - 1)\,\Gamma(1+\alpha), \quad \alpha, \Bbbk \in [0,1]. \tag{3.11}$$

4. Generalized testing

In this section, we generalize the zero-one test by using the fractal trigonometric functions to analyze our results. The zero-one test is formulated by proposing by Gottwald and Melbourne [33–35]. In view of Proposition 1, we select the solution

$$x_n = \frac{1}{\Gamma(1+\alpha)} \sum_{j=0}^{n-1} \Big(1 - \wp\, \hbar_{\mathbb{k}}(x_j) + y_j - x_j\Big),$$
$$y_n = \frac{1}{\Gamma(1+\alpha)} \sum_{j=0}^{n-1} \Big(\ell\, x_j - y_j\Big).$$

Define two translation terms

$$\rho_n = \sum_{j=0}^{n-1} x_n \cos_\alpha(j\tau^\alpha),$$
$$\varrho_n = \sum_{j=0}^{n-1} x_n \sin_\alpha(j\tau^\alpha).$$

Next, we formulate the fractal square displacement for x_n, where the control law is defined $\mu_\tau(n)$ by:

$$\mu_\tau(n) = \lim_{N\to\infty} \frac{1}{N} \sum_{j=0}^{N-1} \Big(\rho_{n+j} - \rho_j\Big)^2 + \Big(\varrho_{n+j} - \varrho_j\Big)^2.$$

Hence, the asymptotic growth is formulated by

$$G_\tau := \lim_{n\to\infty} \Big|\frac{\log \mu_\tau(n)}{\log(n)}\Big|.$$

Obviously, the asymptotic growth ratio approaches to zero in the ordinary case, while heads for one in the chaotic case. For $\alpha = 1$ (the ordinary case), we have the generalized Puiseux series by

$$G_\tau \approx \frac{\log(2 - 2\cos(1))}{\log(n)} + O((\frac{1}{n})^2) \approx 0.$$

For all $\alpha \in (0, 1)$, the gamma function can be approximated by

$$\Gamma(\chi) = \frac{1}{\chi} - \gamma + \tfrac{1}{2}\left(\gamma^2 + \frac{\pi^2}{6}\right)\chi - \tfrac{1}{6}\left(\gamma^3 + \frac{\gamma\pi^2}{2} + 2\zeta(3)\right)\chi^2 + O(\chi^3),$$

where γ is the Euler number and ζ is the zeta function. Thus we obtain the (see Figure 6)

$$G_\tau = \Big|\frac{\log(1/n)}{\log(n)}\Big| = 1.$$

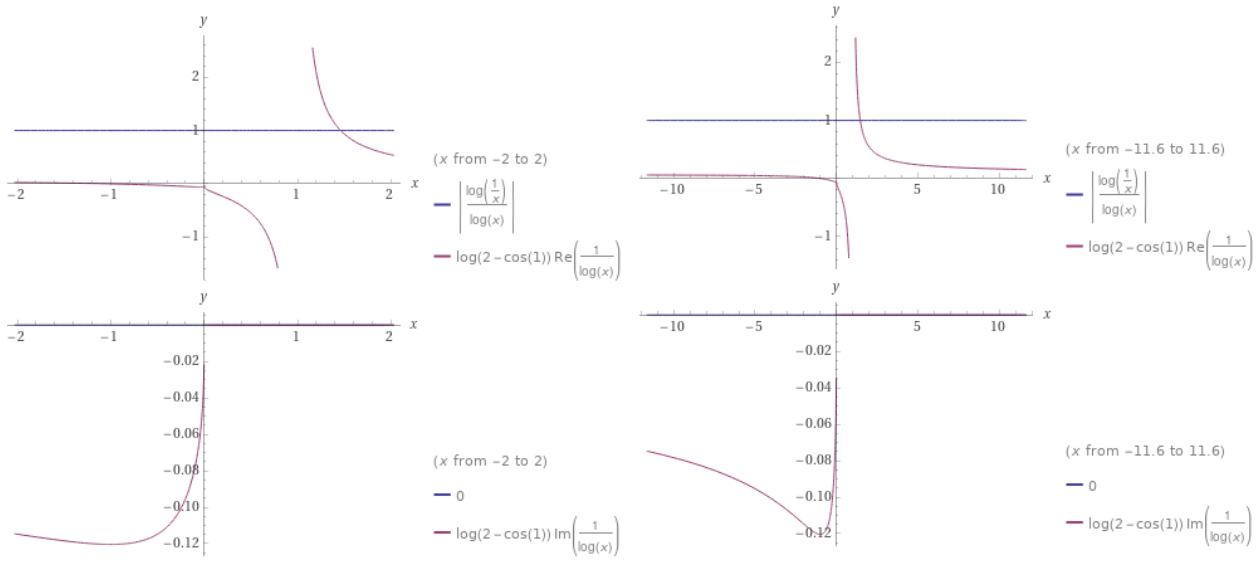

Figure 6. The plot of G_μ, the red one is the ordinary case, which tends to zero, the blue one is for the fractal case which tends to one.

5. Conclusions

A new fractal-order chaotic map has been devised, displaying a variety of marvels such as chaos and synchronized attractions. The Yong-like difference operator was used to analyze the FHLS map. Bifurcation graphs have been provided for both α and $\Bbbk$ parameters. The FHLS map rests chaotic across a wide range of parameter space, as a result of the consequences. The existence of solutions is discussed using the system's fixed points; the necessary requirements for stability are shown; and lastly, the system was tested for convergence. As a result, it has a lot of applications in the engineering field, such as transistors, resistors, conductors, capacitors, and diodes in an electrical circuit. Furthermore, a spectacular 1D-control legislation for stabilizing the conditions of the recommended map was established. The fixed point theory indicates that there is global stability. The generalized zero-one test is used to assess the stability of solutions and provides testing. As future works, we aim to consider two different four parameters dimensional dynamical systems with Caputo fractional derivative or its modifications. In this case, the control system will be studied as 2D-system.

Conflict of interest

The authors declare no conflict of interest.

References

1. M. Hénon, A two-dimensional mapping with a strange attractor, *Commun.Math. Phys.*, **50** (1976), 69–77. http://dx.doi.org/10.1007/BF01608556
2. S. Strogatz, *Nonlinear dynamics and chaos: with applications to physics, biology, chemistry and engineering*, Boca Raton: CRC press, 2018.
3. Z. Elhadj, J. Sprott, A unified piecewise smooth chaotic mapping that contains the Hénon and the Lozi systems, *Annual Review of Chaos Theory, Bifurcations and Dynamical Systems*, **1** (2011), 50–60.
4. A. Ouannas, A. Khennaoui, X. Wang, V. Pham, S. Boulaaras, S. Momani, Bifurcation and chaos in the fractional form of Hénon-Lozi type map, *Eur. Phys. J. Spec. Top.*, **229** (2020), 2261–2273. http://dx.doi.org/10.1140/epjst/e2020-900193-4
5. K. Kolwankar, A. Gangal, Fractional differentiability of nowhere differentiable functions and dimensions, *Chaos*, **6** (1996), 505. http://dx.doi.org/10.1063/1.166197
6. X. Yang, D. Baleanu, H. Srivastava, *Local fractional integral transforms and their applications*. Pittsburgh: Academic Press, 2016. http://dx.doi.org/10.1016/C2014-0-04768-5
7. X. Yang, D. Baleanu, H. Srivastava, Local fractional similarity solution for the diffusion equation defined on Cantor sets, *Appl. Math. Lett.*, **47** (2015), 54–60. http://dx.doi.org/10.1016/j.aml.2015.02.024
8. C. Cattani, H. Srivastava, X. Yang, *Fractional dynamics*, Warsaw: De Gruyter Open Poland, 2015. http://dx.doi.org/10.1515/9783110472097
9. V. Basharan, W. Siluvairaj, M. Velayutham, Recognition of multiple partial discharge patterns by multi-class support vector machine using fractal image processing technique, *IET Sci. Meas. Technol.*, **12** (2018), 1031–1038. http://dx.doi.org/10.1049/iet-smt.2018.5020
10. K. Jena, S. Mishra, S. Mishra, An edge detection approach for fractal image processing, In: *Examining fractal image processing and analysis*, Hershey: IGI Global, 2020, 1–22. http://dx.doi.org/10.4018/978-1-7998-0066-8.ch001
11. P. Chowdhury, P. Shivakumara, H. Jalab, R. Ibrahim, U. Pal, T. Lu, A new fractal series expansion based enhancement model for license plate recognition, *Signal Process.-Image*, **89** (2020), 115958. http://dx.doi.org/10.1016/j.image.2020.115958
12. A. Al-Shamasneh, H. Jalab, S. Palaiahnakote, U. Obaidellah, R. Ibrahim, M. El-Melegy, A new local fractional entropy-based model for kidney MRI image enhancement, *Entropy*, **20** (2018), 344. http://dx.doi.org/10.3390/e20050344
13. Y. Chen, Y. Long, Spatial signal analysis based on wave-spectral fractal scaling: a case of urban street networks, *Appl. Sci.*, **11** (2021), 87. http://dx.doi.org/10.3390/app11010087
14. Z. Elhadj, *Dynamical systems: theories and applications*, Boca Raton: CRC Press, 2019. http://dx.doi.org/10.1201/9780429028939
15. R. Matousek, R. Lozi, T. Hulka, Stabilization of higher periodic orbits of the Lozi and Hénon maps using meta-evolutionary approaches, *Proceedings of IEEE Congress on Evolutionary Computation (CEC)*, 2021, 572–579. http://dx.doi.org/10.1109/CEC45853.2021.9504798

16. E. Bonyah, M. Yavuz, D. Baleanu, S. Kumar, A robust study on the listeriosis disease by adopting fractal-fractional operators, *Alex. Eng. J.*, **61** (2022), 2016–2028. http://dx.doi.org/10.1016/j.aej.2021.07.010

17. S. Qureshi, R. Jan, Modeling of measles epidemic with optimized fractional order under Caputo differential operator, *Chaos Soliton. Fract.*, **145** (2021), 110766. http://dx.doi.org/10.1016/j.chaos.2021.110766

18. K. Sadri, K. Hosseini, D. Baleanu, S. Salahshour, C. Park, Designing a matrix collocation method for fractional delay integro-differential equations with weakly singular kernels based on Vieta-Fibonacci polynomials, *Fractal Fract.*, **6** (2022), 2. http://dx.doi.org/10.3390/fractalfract6010002

19. S. Qureshi, M. Chang, A. Shaikh, Analysis of series RL and RC circuits with time-invariant source using truncated M, Atangana beta and conformable derivatives, *J. Ocean Eng. Sci.*, **6** (2021), 217–227. http://dx.doi.org/10.1016/j.joes.2020.11.006

20. A. Yusuf, S. Qureshi, U. Mustapha, S. Musa, T. Sulaiman, Fractional modeling for improving scholastic performance of students with optimal control, *Int. J. Appl. Comput. Math.*, **8** (2022), 37. http://dx.doi.org/10.1007/s40819-021-01177-1

21. S. Qureshi, Fox H-functions as exact solutions for Caputo type mass spring damper system under Sumudu transform, *J. Appl. Math. Comp. Mec.*, **20** (2021), 83–89. http://dx.doi.org/10.17512/jamcm.2021.1.08

22. X. Li, Y. Wang, M. Khan, M. Alshahrani, T. Muhammad, A dynamical study of SARS-COV-2: a study of third wave, *Results Phys.*, **29** (2021), 104705. http://dx.doi.org/10.1016/j.rinp.2021.104705

23. Z. Shen, Y. Chu, M. Khan, S. Muhammad, O. Al-Hartomy, M. Higazy, Mathematical modeling and optimal control of the COVID-19 dynamics, *Results Phys.*, **31** (2021), 105028. http://dx.doi.org/10.1016/j.rinp.2021.105028

24. X. Li, N. Gul, M. Khan, R. Bilal, A. Ali, M. Alshahrani, A new Hepatitis B model in light of asymptomatic carriers and vaccination study through Atangana-Baleanu derivative, *Results Phys.*, **29** (2021), 104603. http://dx.doi.org/10.1016/j.rinp.2021.104603

25. P. Xiong, M. Ijaz Khan, R. Punith Gowda, R. Naveen Kumar, B. Prasannakumara, Y. Chu, Comparative analysis of (Zinc ferrite, Nickel Zinc ferrite) hybrid nanofluids slip flow with entropy generation, *Mod. Phys. Lett. B*, **35** (2021), 2150342. http://dx.doi.org/10.1142/S0217984921503425

26. P. Xiong, A. Hamid, Y. Chu, M. Ijaz Khan, R. Gowda, R. Naveen Kumar, et al., Dynamics of multiple solutions of Darcy-Forchheimer saturated flow of cross nanofluid by a vertical thin needle point, *Eur. Phys. J. Plus*, **136** (2021), 315. http://dx.doi.org/10.1140/epjp/s13360-021-01294-2

27. T. Abdeljawad, A. Atangana, J. Gómez-Aguilar, F. Jarad, On a more general fractional integration by parts formulae and applications, *Physica A*, **536** (2019), 122494. http://dx.doi.org/10.1016/j.physa.2019.122494

28. A. Khan, H. Khan, J. Gómez-Aguilar, T. Abdeljawad, Existence and Hyers-Ulam stability for a nonlinear singular fractional differential equations with Mittag-Leffler kernel, *Chaos Soliton. Fract.*, **127** (2019), 422–427. http://dx.doi.org/10.1016/j.chaos.2019.07.026

29. P. Bedi, A. Kumar, T. Abdeljawad, A. Khan, J. Gomez-Aguilar, Mild solutions of coupled hybrid fractional order system with Caputo-Hadamard derivatives, *Fractals*, **29** (2021), 2150158. http://dx.doi.org/10.1142/S0218348X21501589

30. H. Khan, T. Abdeljawad, J. Gomez-Aguilar, H. Tajadodi, A. Khan, Fractional order Volterra integro-differential equation with Mittag-Leffler kernel, *Fractals*, **29** (2021), 2150154. http://dx.doi.org/10.1142/S0218348X21501541

31. O. Martínez-Fuentes, F. Meléndez-Vázquez, G. Fernández-Anaya, J. Gómez-Aguilar, Analysis of fractional-order nonlinear dynamic systems with general analytic kernels: Lyapunov stability and inequalities, *Mathematics*, **9** (2021), 2084. http://dx.doi.org/10.3390/math9172084

32. Asma, J. Gómez-Aguilar, G. Rahman, M. Javed, Stability analysis for fractional order implicit ψ-Hilfer differential equations, *Math. Method. Appl. Sci.*, **45** (2022), 2701–2712. http://dx.doi.org/10.1002/mma.7948

33. G. Gottwald, I. Melbourne, A new test for chaos in deterministic systems, *Proc. R. Soc. Lond. A.*, **460** (2004), 603–611. http://dx.doi.org/10.1098/rspa.2003.1183

34. G. Gottwald, I. Melbourne, On the implementation of the 0-1 test for chaos, *SIAM J. Appl. Dyn. Syst.*, **8** (2009), 129–145. http://dx.doi.org/10.1137/080718851

35. G. Gottwald, I. Melbourne, The 0-1 test for chaos: a review, In: *Lecture notes in physics*, Berlin: Springer, 2016, 221–247. http://dx.doi.org/10.1007/978-3-662-48410-4_7

AIMS Press